THE JOURNAL OF PHYSICAL CHEMISTRY B

Article

pubs.acs.org/JPCB

Structural Models for Cu(II) Bound to the Fragment 92−96 of the Human Prion Protein

Rafael Grande-Aztatzi, Lina Rivillas-Acevedo, Liliana Quintanar,* and Alberto Vela*

Departamento de Química, Cinvestav, Av. IPN 2508, San Pedro Zacatenco, México, D.F., 07360, México

Supporting Information

ABSTRACT: The prion protein (PrP^C) binds Cu(II) in its N-terminal region, and it is associated to a group of neurodegenerative diseases termed transmissible spongiform encephalopaties (TSEs). The isoform PrP^{Sc}, derived from the normal PrP^C, is the pathogenic agent of TSEs. Using spectroscopic techniques (UV−vis absorption, circular dichroism, and electron paramagnetic resonance) and electronic structure calculations, we obtained a structural description for the different pH-dependent binding modes of Cu(II) to the PrP(92−96) fragment. We have also evaluated the possibility of water molecule ligation to the His96-bound copper ion. Geometry-optimized structural models that reproduce the spectroscopic features of these complexes are presented. Two Cu(II) binding modes are relevant at physiological pH: 4N and 3NO equatorial coordination modes; these are best described by models with no participation of water molecules in the coordination sphere of the metal ion. In contrast, the 2N2O and N3O coordination modes that are formed at lower pH involve the coordination of an axial water molecule. This study underscores the importance of including explicit water molecules when modeling copper binding sites in PrP^C.

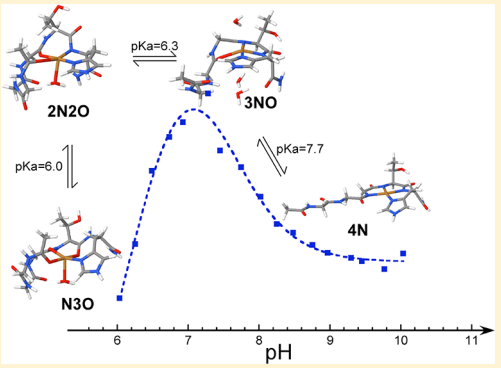

I. INTRODUCTION

The prion protein (PrP) is a membrane-anchored glycoprotein that has been associated to a group of invariably fatal neurodegenerative diseases called transmissible spongiform encephalopaties (TSEs), which include scrapie in goats and sheep, mad cow disease, chronic wasting disease in deer and elk, and Creutzfeldt-Jakob disease in humans. TSEs are mediated by an entirely novel mechanism, which involve modification of the normal cellular protein (PrP^C) into the abnormal infectious isoform (PrP^{Sc}). Unlike the PrP^C isomer, PrP^{Sc} is rich in β-sheet structure, is highly insoluble, is protease-resistant, and readily forms aggregates and amyloid fibrils. These aggregates lead to the formation of neuronal plaques that have been associated to the induction of neuron apoptosis.[1−3] The specific function of PrP^C has not been completely unraveled, but it is known that its N-terminal domain binds copper in vivo.[4,5] Thus, it has been proposed that PrP^C participates in copper homeostasis or uptake into the cell.[6,7] Other studies have proposed a copper-dependent antioxidant function,[8,9] a role as superoxide dismutase,[10] its involvement in cell−cell adhesion,[11] signal transduction,[12] as an antiapoptosis agent,[13] and for the modulation of *N*-methyl-D-aspartate (NMDA) receptor's activity.[14]

PrP^C is formed by a predominantly α-helical C-terminal domain and an unstructured N-terminal domain,[15] where six Cu ions can bind,[16,17] four of them to the octarepeat region, which contains the highly conserved octapeptide PHGGGWGQ (residues 60−91 in the human sequence). The other two Cu ions bind to His96 and His111, which have been identified as binding anchors in the region spanning residues 92−115.[16−20] The octarepeat region binds copper in a series of different coordination modes, depending on pH and the relative concentration of copper to protein.[21] When there is enough Cu(II), each octarepeat fragment binds one Cu ion through HGGGW residues with a 3NO equatorial coordination mode at physiological pH; the coordinating atoms are provided by the His imidazole ring, the deprotonated amide nitrogens of the two following Gly residues, and a backbone carbonyl oxygen. A water molecule coordinates in the axial position.[16,22] On the other hand, the PrP(92−96) and PrP(106−113) fragments have been identified as the minimal sequences to reproduce Cu(II) binding to His96 and His111, respectively.[17,19,23] Controversy still exists about coordination modes in the full protein, since some studies identify either His96[16,18] or His111[17,19,24−28] as the sites with the highest affinity, while others suggest that Cu(II) binds to each His site with equal affinity.[29] However, the formation of a Cu(II) complex involving both His residues cannot be ruled out, particularly at low pH and low Cu:protein ratios.[30]

Early electron paramagnetic resonance (EPR) studies clearly demonstrated that Cu(II) coordination to the PrP(92−96) fragment involves the His96 imidazole and deprotonated amide groups from the preceding Thr and Gly residues.[17] Thus, an important difference between this coordination site and the

Received: October 9, 2012
Revised: December 10, 2012
Published: December 14, 2012

octarepeat region is that the His96 Cu binding site involves amide groups that precede the His residue in the sequence. It was also demonstrated that the coordination is highly pH-dependent, and at physiological pH, the 3NO and 4N equatorial coordination modes are relevant.[31,32] It has been proposed that the 3NO mode involves the His96 imidazole ring, two deprotonated amides, and a backbone carbonyl, while, in the 4N mode, the latter is replaced by a third deprotonated amide.

The electronic structure of the His96 Cu binding site has been relatively unexplored in theoretical studies.[33−36] The lack of a crystal structure for this coordination site makes the construction of appropriate structural models challenging. Thus, the comparison of calculated spectroscopic parameters with experimental data becomes crucial for validating different coordination models. An earlier study has reported the simulation of circular dichroism (CD) spectra for Cu(II) complexes with a GGGH model in a 4N coordination mode;[33] however, the comparison to experimental data showed large differences, possibly due to the fact that the model does not correspond to the actual sequence for this binding site, and/or because the role of explicit water molecules was not taken into account. Recently, the calculation of EPR parameters and their comparison to experimental data has proved useful in identifying the best coordination model for Cu binding to His111.[37]

In this study, different spectroscopic techniques are used (UV−vis absorption, CD, and EPR) in combination with electronic structure calculations to evaluate the proposed coordination modes of Cu(II) binding to the GGGTH sequence of the PrP(92−96) fragment. EPR parameters, electronic absorption, and CD spectra are calculated for several different coordination models, to compare to experimental data. The effect of explicit water molecules is also evaluated.

II. MATERIALS AND METHODS

All chemicals were reagent grade and used without further purification. Water was purified to a resistivity of 18 MΩ/cm using a Millipore Gradient deionizing system.

Peptide Preparation and Concentration Determination. The PrP(92−96) fragment with sequence GGGTH, acetylated at the N-terminus and amidated at the C-terminus, was purchased from Peptides International. Peptide solutions were prepared in 10 mM 2-(*N*-morpholino)ethanesulfonic acid (MES) buffer for pH 6.5, in 10 mM *N*-ethylmorpholine (NEM) for pH 7.5 and 8.5, or in a mixture of both buffers for pH dependence studies. For the pH titrations, the pH was varied every 0.25 units by adding small volumes of NaOH or HCl solutions. Peptide samples for EPR spectroscopy were prepared in buffers with 50% glycerol to achieve adequate glassing. The addition of glycerol has no effect in the structure of the Cu(II)−peptide complexes, as evaluated by absorption and CD spectroscopy for all buffer solutions and pH values used in this study. The absorption coefficient for the peptide at 214 nm was determined in each buffer solution at pH 6.5, 7.5, and 8.5, and it was found to be buffer- and pH-independent. This absorption coefficient was used to determine the final concentration of peptide in each sample that was analyzed (approximately 0.5 mM).

UV−Visible Absorption and Circular Dichroism Spectroscopy. Room temperature absorption and CD spectra were recorded using an Agilent 8453 diode array spectrometer and a Jasco J-815 CD spectropolarimeter, respectively. Spectra were recorded in quartz cells with either 1 or 0.1 cm path lengths. Gaussian fitting of the absorption and CD spectra was performed using PeakFit 4.0 (Jandel), keeping the same parameters (energy and bandwidth) for individual Gaussian bands for both the absorption and CD spectra. The minimum number of bands was used to adequately fit key features in both spectra.

Electron Paramagnetic Resonance Spectroscopy. X-band EPR spectra were collected using an EMX Plus Bruker System, with an ER 041 XG microwave bridge and an ER 4102ST cavity. The following conditions were used: microwave power, 10 mW; modulation amplitude, 5 G; modulation frequency, 100 kHz; time constant, 327 ms; conversion time, 82 ms; and averaging over 18 scans. X-Band EPR spectra were recorded at 150 K using an ER4131VT variable temperature nitrogen system. For experiments performed in ^{17}O water, the buffer solution (10 mM MES) was prepared with 60−70% enriched $H_2{}^{17}O$ (Cambridge Isotopes) and 30% glycerol to achieve adequate glassing. The peptide was dissolved in this solution at a final concentration of 1 mM, 0.5 equivalents of Cu(II) were added, and the pH of the final solution was adjusted using a microelectrode and a solution of NaOH in 60−70% enriched $H_2{}^{17}O$. A peptide sample in ^{16}O water was prepared in parallel using the same protocol for each experiment, and the same conditions described. EPR spectra were baseline-corrected and analyzed using WinEPR SimFonia (Bruker).

Electronic Structure Calculations. All models use the sequence GGGTH of the PrP(92−96) fragment, with the N- and C-terminals acetylated and amidated, respectively. Each Cu(II)−peptide complex was constructed in Molden,[38] and the electronic structure was obtained using spin-unrestricted Kohn−Sham theory (UKS) and within the linear combination of Gaussian-type orbitals to solve the Kohn−Sham equations (LCGTO-KS)[39] as implemented in the deMon2k code.[40] All structures with a spin multiplicity of two (doublet) were fully optimized without any geometry constraints at local level (LDA) with the Dirac[41]-VWN[42] exchange-correlation functional and then with the nonempirical generalized gradient approximation (GGA) exchange-correlation functional PBE[43] that belongs to the second rung of Jacobs' ladder,[44] using a double-ζ with polarization (DZVP)[45] orbital basis set and an automatically generated GEN-A2 auxiliary basis set. The auxiliary set is used to avoid the evaluation of four center integrals by invoking the variational fitting of the Coulomb energy.[46,47] The stationary points were characterized by a frequency analysis that was done with the PBE functional. The optimized structures were used to calculate the EPR parameters, **g** and **A** tensors, with the ORCA program,[48] using the nonempirical global hybrid functional PBE0[49] with the CP[50] basis for copper and the DGAUSS[45] basis in all other atoms. IGLO[51] was used as the gauge origin and spin−orbit coupling was included. To simulate the UV−vis absorption and CD spectra, time-dependent density functional theory (TD-DFT) calculations were performed with the same nonempirical global hybrid functional and a triple-ζ with polarization (TZVP)[52] basis set. Fifty roots were calculated. In all cases, solvent effects were included using the implicit solvation model COSMO.[53,54] The spectra were simulated summing Gaussians centered at each calculated root using a full width at half-maximum (fwhm) for all excitations of 500, 1500, 3000, or 5000 cm^{-1}. The lines representing bonds or bonding schemes depicted in the figures were obtained by comparing the

dx.doi.org/10.1021/jp310000h | J. Phys. Chem. B 2013, 117, 789−799

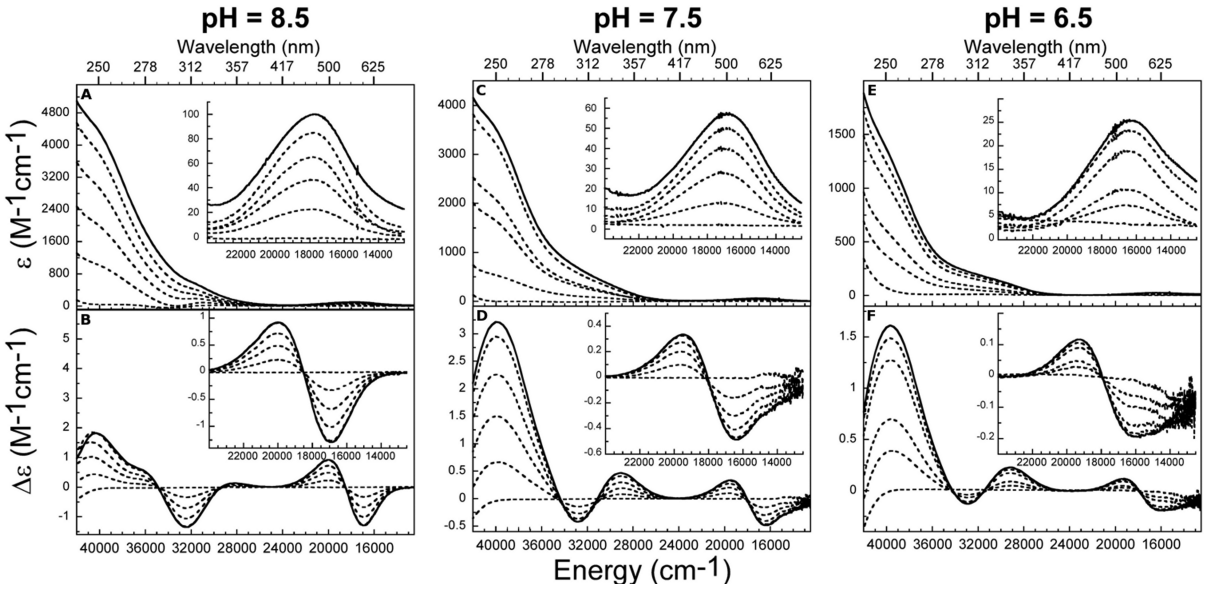

Figure 1. Titration of the PrP(92−96) fragment with Cu(II) as followed by UV−vis absorption at pH 8.5 (A), 7.5 (C), and 6.5 (E) and by circular dichroism at pH 8.5 (B), 7.5 (D), and 6.5 (F). Only the spectra recorded after the addition of 0, 0.2, 0.4, 0.6, and 0.8 equiv (all in dotted lines) and 1.0 equiv (solid lines) of Cu(II) are displayed. A blow-up of the lower energy region is shown in the inset for each figure.

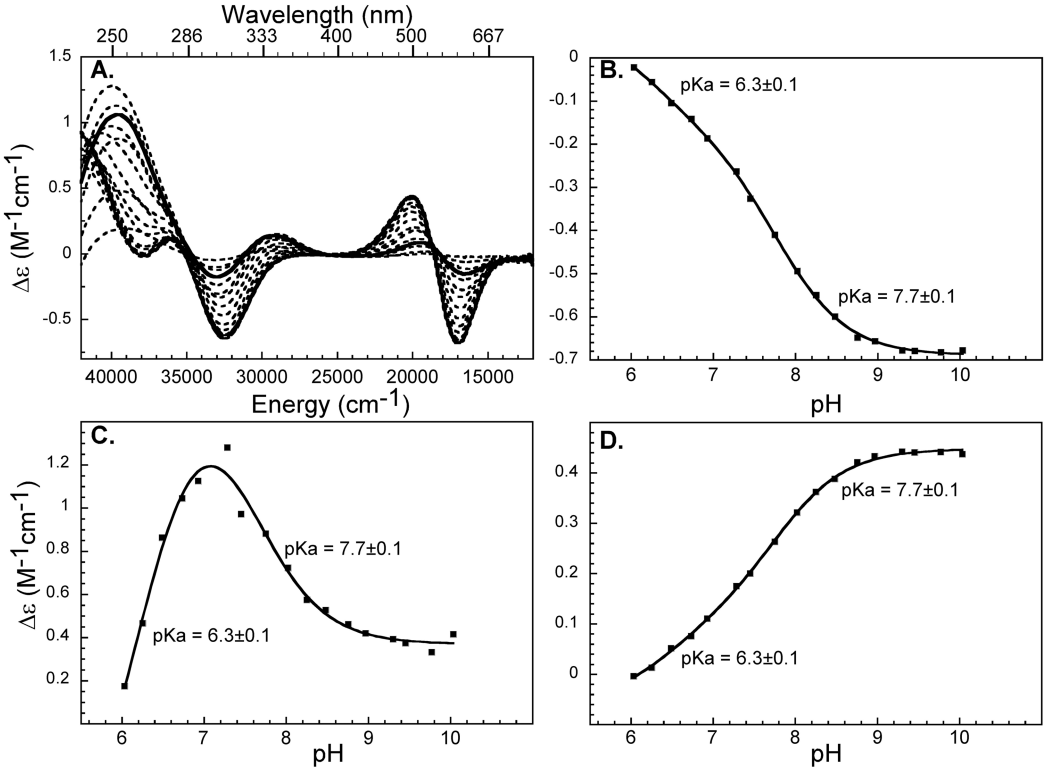

Figure 2. pH titration of the Cu(II)−PrP(92−96) complex (A), as followed by circular dichroism. The Cu(II) complex was titrated from pH ∼ 6.0 to pH ∼ 10 (dashed bold line); spectra for intermediate pH values are shown in dashed lines, except for pH 6.7 (continuous bold line). The traces for the CD signal intensity changes at 16949 cm^{-1} (B), 40000 cm^{-1} (C), and 20080 cm^{-1} (D) for the Cu(II) complex with PrP(92−96) were fit to the model described in the text (solid lines) to determine the associated pK_a.

distances between any two atoms with the sum of their van der Walls radii.

III. RESULTS AND DISCUSSION

III.1. Spectroscopic Study of Cu(II) Binding to the PrP(92−96) Fragment. The PrP(92−96) fragment was titrated with Cu(II) at three different pH values 6.5, 7.5, and 8.5, and the titration was followed simultaneously by UV−vis absorption and CD. All signals saturate after 1 equiv of Cu(II) has been added (data not shown). The absorption data at pH 8.5 (Figure 1A) show the growth of a high intensity ($\varepsilon \approx 4800$ M^{-1} cm^{-1}) signal at ∼39700 cm^{-1}, a shoulder at ∼32000 cm^{-1}, and a low intensity broad band ($\varepsilon \approx 100$ $M^{-1}cm^{-1}$) centered at 17700 cm^{-1} upon addition of Cu(II). The absorption spectrum

dx.doi.org/10.1021/jp310000h | J. Phys. Chem. B 2013, 117, 789−799

of a metal complex can display ligand field (d−d) and charge transfer transitions.[55] The latter ones are usually electric dipole allowed and display high intensity, such as the signal at ∼39700 cm^{-1} in Figure 1A. In contrast, the d−d transitions appear in the lower energy region of the spectrum and they are electric dipole forbidden, and, thus, display small ε values, such as the signal observed at 17700 cm^{-1}. For chiral complexes, such as metal−peptide complexes, CD spectroscopy can probe the same electronic transitions that are observed by absorption. The CD spectrum of the Cu(II)−PrP(92−96) complex at pH 8.5 (Figure 1B) displays a broad signal at ∼41600 cm^{-1} ($\Delta\varepsilon \approx 2\ M^{-1}\ cm^{-1}$) with a shoulder at 36200 cm^{-1} and a less intense ($\Delta\varepsilon \approx 0.7\ M^{-1}\ cm^{-1}$) band at 32500 cm^{-1}; these correspond to charge transfer transitions that contribute to the intense signals observed in the absorption spectrum. In a CD spectrum, signals can be positive or negative, depending on the Cotton effect of the electronic transitions.[56,57] Thus, two transitions that overlap in the absorption spectrum can be deconvoluted by CD; this is the case of the broad low intensity absorption band at 17700 cm^{-1} (Figure 1A, inset) that gets resolved by CD into a positive signal at 19500 cm^{-1} and a negative signal at 17000 cm^{-1} (Figure 1B, inset).

Titration of the PrP(92−96) fragment with Cu(II) at pH 7.5 (Figure 1C and D) displays similar signals as those observed at pH 8.5 but with lower intensity. A new positive band at 29000 cm^{-1} becomes more evident in the CD spectrum, while the positive signals above 36000 cm^{-1} gain intensity at pH 7.5 as compared to pH 8.5. In the d−d region, the absorption band shifts to lower energy (Figure 1C, inset), and a shoulder at 13900 cm^{-1} becomes evident in the CD spectrum (Figure 1D, inset). Finally, titration of the PrP(92−96) fragment with Cu(II) at pH 6.5 (Figure 1E and F) displays practically the same signals as those observed at pH 7.5 but with lower intensity.

In order to further evaluate the changes observed in the CD spectra of the Cu(II)−PrP(92−96) complex upon pH, 1 equiv of Cu(II) was added to a 0.5 mM solution of the peptide, and a pH titration of the solution was followed by CD in a range of pH from 5.7 to 10. Figure 2A shows clearly the CD spectral changes associated to the variation of pH. The spectral changes at 16950, 20080, and 40000 cm^{-1} (Figure 2B and D) make evident the presence of two protonation states. The experimental data at the three energy values could be best fit with the following model:

$$\Delta\varepsilon_{obs} = \frac{(\Delta\varepsilon_1[H^+]^2 + \Delta\varepsilon_2[H^+]Ka_1 + \Delta\varepsilon_3 Ka_1 Ka_2)}{[H^+]^2 + [H^+]Ka_1 + Ka_1 Ka_2}$$

where $\Delta\varepsilon_{obs}$ is the observed CD signal intensity at any given pH, Ka_1 and Ka_2 are equilibrium constants associated to the two protonation states of the Cu(II)−peptide complex, and $\Delta\varepsilon_1$, $\Delta\varepsilon_2$, and $\Delta\varepsilon_3$ are the CD signal intensities of the three different species with different protonation states. The pK_a values associated to the two protonation equilibria of the Cu(II)−PrP(92−96) complex are 6.3 ± 0.1 and 7.7 ± 0.1, as determined by the best fit of experimental data derived from at least triplicate experiments. These values are in agreement with previously reported pK_a values, as derived from potentiometric experiments.[31]

At physiological pH, the dominating species are the two protonation states of the Cu(II)−PrP(92−96) complex that are associated to the pK_a of 7.7. In order to further characterize these two forms, simultaneous Gaussian analysis of the absorption and CD spectra at pH 7.0 and pH 9.0 was performed. The absorption and CD spectra, at both pH values, can be resolved into six transitions with the energies listed in Table 1, and shown in Figure 3. On the basis of their high Kuhn anisotropy factors (ratio of CD to absorption intensity, $\Delta\varepsilon/\varepsilon$, Table 1), bands 1−3 can be assigned as ligand field (d−d) transitions, while bands 4−6 can be assigned as ligand-to-metal charge transfer (LMCT) transitions. Three d−d transitions are needed to fit both the absorption and CD spectra, consistent with having a Cu(II) complex with a distorted square planar geometry. At pH 9.0, the maximum λ and absorption extinction coefficient are ∼18000 cm^{-1} and ∼80 $M^{-1}\ cm^{-1}$, respectively (Figure 3A), consistent with a Cu(II) coordination environment involving a His residue and three deprotonated amide groups.[58,59] Studies of tetracoordinated Cu(II)−imidazole and Cu(II)−peptide complexes have shown that the interaction with the imidazole nitrogen is expected to generate two $\pi \rightarrow$ Cu(II) charge transfer (CT) transitions ($\pi_1 \rightarrow$ Cu(II) CT at 27000 to 35700 cm^{-1} and $\pi_2 \rightarrow$ Cu(II) CT at 32500 to 40800 cm^{-1}).[60,61] Moreover, Cu(II) coordination by deprotonated backbone amide groups generates a $N^- \rightarrow$ Cu(II) CT transition at 31000 to 34000 cm^{-1}.[62−64] Thus, the LMCT bands numbered 5 and 6 in Figure 3 and Table 1 can be assigned to $\pi_1 \rightarrow$ Cu(II) and $\pi_2 \rightarrow$ Cu(II) CT transitions, respectively, derived from Cu coordination by His96, while the LMCT transition number 4 can be assigned to a $N^- \rightarrow$Cu(II) CT transition.

Table 1. Gaussian Fits of Absorption and CD Spectra of GGGTH at pH 9.0 and 7.0 + 1 equiv Cu(II)

	pH 9.0			pH 7.0		
band no.	energy[a]	λ	$\Delta\varepsilon/\varepsilon$[b]	energy	λ	$\Delta\varepsilon/\varepsilon$[b]
1 d → d	17107	585	−32.4	13925	718	−7.32
2 d → d	19546	512	33.5	16711	598	−12.3
3 d → d	21563	464	143.6	19471	514	37.9
4 N^-_{amide} → Cu CT	32481	308	−5.71	29147	343	12.0
5 N π_1 → Cu CT	35780	279	0.358	33071	765	−1.49
6 N π_2 → Cu CT	41635	240	0.444	39608	252	1.15

[a]The energy (cm^{-1}) and wavelength (nm) were obtained from simultaneously fitting the CD and the absorption spectrum. [b]Kuhn anisotropy factor.

The Cu(II) titrations of the PrP(92−96) peptide were also followed by X-band EPR (Supporting Information, Figure S1). In all cases, the EPR spectra display $g_{\|} > g_{\perp} > 2.00$ and a large parallel hyperfine splitting, which is indicative of a $d_{x^2-y^2}$ ground state. The X-band EPR spectrum of the Cu(II) complex with PrP(92−96) at pH 8.5 shows a $g_{\|}$ value of 2.207 and a hyperfine coupling of $A_{\|} = 206 \times 10^{-4}\ cm^{-1} = 617$ MHz (Table 2); these values correspond to a 4N equatorial coordination according to the Peisach−Blumberg correlations.[65] The EPR titration performed at pH 7.0 shows a $g_{\|}$ value of 2.233 and a hyperfine splitting of $A_{\|} = 180 \times 10^{-4}\ cm^{-1} = 541$ MHz; these values fall right in the middle of the two trend lines for the 4N and 2N2O in the Peisach−Blumberg correlations,[65] suggesting a 3NO equatorial coordination mode.

In order to gain insight into the nature of the oxygen donor in the Cu(II)−PrP(92−96) complex at low pH, the complex was prepared in ^{17}O-enriched water. It is well established that

dx.doi.org/10.1021/jp310000h | J. Phys. Chem. B 2013, 117, 789−799

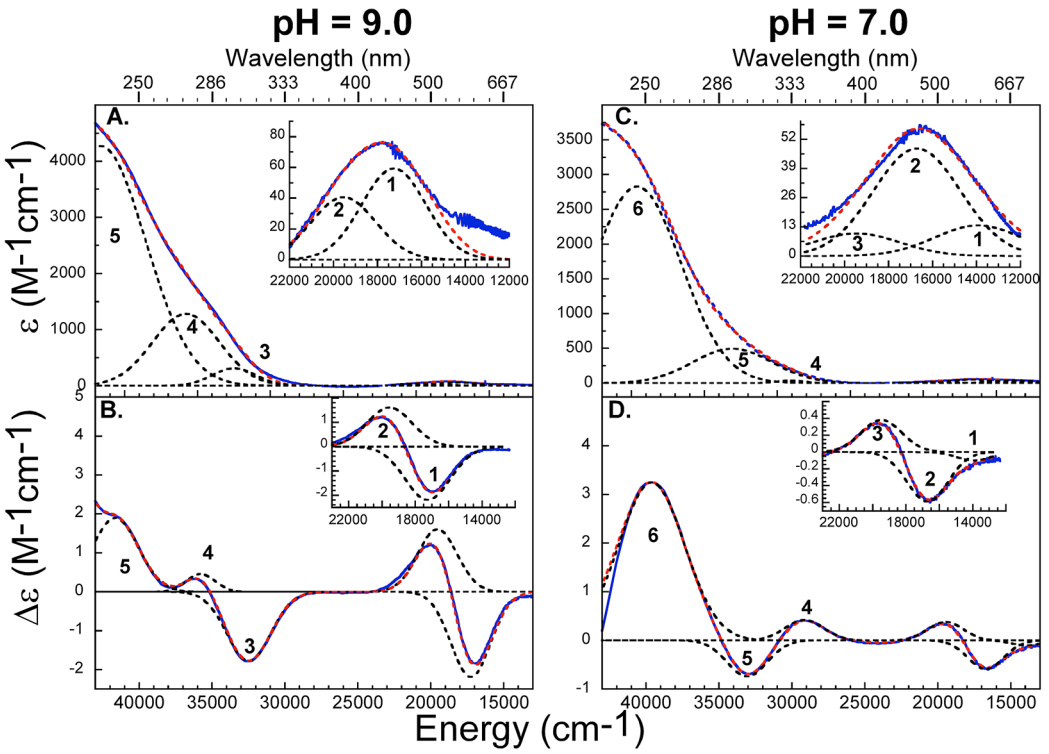

Figure 3. Gaussian fits of the UV−vis absorption (A and C) and circular dichroism (B and D) spectra of the Cu(II)−PrP(92−96) complex at pH 9.0 and 7.0, respectively. The peptide spectra without Cu(II) were subtracted in all cases. Experimental spectra (blue), Gaussian fits (red), and individual Gaussian bands (dotted lines) with the parameters listed in Table 1 are shown.

the superhyperfine coupling of the ^{17}O nucleus of a water molecule coordinated to Cu(II) in the equatorial position leads to significant line broadening in the EPR signal of the complex.[66,67] A comparison of the X-band EPR spectra of the Cu(II)−PrP(92−96) complex at pH 7.0 in ^{17}O and in ^{16}O water clearly shows no difference in the line width of the EPR signals (Figure 4). This result suggests that the oxygen atom in the 3NO coordination mode of this complex is not provided by an equatorial water molecule but probably by a backbone carbonyl group, in a similar fashion to that reported for the PHGGGWGQ fragment.[22] This is consistent with HYSCORE, ENDOR, and FT-IR results that suggest that the oxygen ligand in the equatorial position at pH 7.0 is a backbone carbonyl.[22,32] It should be noted that the presence of a water molecule coordinated as an axial ligand cannot be discarded, given that the superhyperfine coupling of the ^{17}O nucleus of a water molecule axially coordinated to Cu(II) tends to be very small[67] and cannot be easily identified with this type of experiment.

III.2. Electronic Structure of Cu(II) Complexes with the PrP(92−96) Peptide. Using UKS calculations, as described in the Materials and Methods section, four models with different protonation states were evaluated with equatorial coordinations 4N, 3NO, 2N2O, and N3O. Also, the effect of explicit water molecules was assessed.

III.2.1. 4N Coordination Mode. The 4N coordination mode has the Cu ion coordinated equatorially to the His96 imidazole nitrogen and the deprotonated amides of the His96, Thr95, and Gly94 residues (Figure 5A). The optimized structural parameters reported in Table 3 show that, independently of the exchange-correlation functional, the coordination geometry is almost square planar and the image of the β-LUMO displays a $3d_{x^2-y^2}$ character, indicating that the unpaired electron is mainly located on the metallic center. According to Löwdin's population analysis (LPA), 63.7% of the spin density is in the copper atom, while the deprotonated amide nitrogen atoms contribute with a total of 27.8% and the imidazole nitrogen with only 4.8%, as expected.[37,68−70]

The EPR parameters calculated for this coordination mode are listed in Table 2. A comparison of the computed EPR parameters for the 4N mode with experimental data shows that they are in excellent agreement with the experimental values measured at pH 8.5, with deviations of 0.02 ppm for g_{zz} and 39 MHz for A_{zz}, which are within the range of error reported for this type of calculations,[37,71−73] indicating that the coordination mode at high pH is 4N. It is noteworthy that several 3NO models yield computed g_{zz} values that are close to the experimental number at pH 8.5, but those models give A_{zz} values that are about 100 MHz lower than the experimental A_{zz} (Table 2). Furthermore, the calculated UV−vis absorption and CD spectra (Figure 6) show a good qualitative agreement with the experimental ones. The computed absorption spectrum has a maximum at ∼40000 cm^{-1} with a shoulder at ∼33000 cm^{-1} and the d−d band centered at 19869 cm^{-1} (blue line, Figure 6A), while the CD spectrum displays a positive signal at 20607 cm^{-1} and a negative one at 15923 cm^{-1} (blue line, Figure 6B). The electronic transitions that contribute to the d−d region of the spectra are listed in Table 4. LPA of the molecular orbitals with the major participation in these electronic transitions shows that transitions 2, 3, and 4 are mainly metallic with >35% of copper contribution (Table 4). The theoretical results are in good agreement with the energy of the transitions obtained from the Gaussian fit of the experimental spectra (Table 1), with deviations in the range 200−1500 cm^{-1}.

III.2.2. 3NO Coordination Mode. In the 3NO coordination mode, the Cu ion is coordinated equatorially to the His96 imidazole nitrogen, the deprotonated amides of His96 and

dx.doi.org/10.1021/jp310000h | J. Phys. Chem. B 2013, 117, 789−799

Table 2. Experimental and Computed EPR Parameters for the Cu(II)−PrP(92−96) Complexes with Different Coordination Modes (CM)[b]

		g			A		
pH	CM	g_{xx}	g_{yy}	g_{zz}	A_{xx}	A_{yy}	A_{zz}
8.5	4N			2.207			617 (206)
7.5	4N/3NO			2.212			589 (196)
7.0	3NO			2.233			541 (180)
6.0[a]	N3O[a]			2.36			421 (140)
	4N	2.0471	2.0560	2.1820	4.73	−37.17	−577.95
ID							
0x	3NO	2.0393	2.0817	2.1983	59.24	157.27	−428.64
1a	3NO	2.0490	2.0726	2.2005	44.50	114.97	−476.07
1b	$3NO_w$	2.0483	2.0552	2.1868	4.33	−11.04	−557.34
2a	3NO	2.0469	2.0772	2.2035	14.30	102.44	−494.41
2b	3NO	2.0499	2.0702	2.2005	43.09	104.78	−480.82
3a	$3NOO_w$	2.0449	2.1009	2.2158	−7.89	160.03	−474.63
3b	3NO	2.0479	2.0760	2.2053	10.07	95.04	−501.14
3c	$3NOO_w$	2.0479	2.0839	2.2076	34.38	135.88	−467.76
3d	3NO	2.0508	2.0655	2.1987	24.02	73.68	−512.22
4a	3NO	2.0465	2.0836	2.2053	33.41	129.94	−466.87
4b	$3NOO_w$	2.0529	2.0822	2.2143	−15.44	81.36	−520.02
4c	$3NO_w$	2.0448	2.0651	2.1969	18.92	86.69	−494.86
4d	3NO	2.0511	2.0701	2.2020	41.25	96.63	−488.79
0x	2N2O	2.0583	2.0655	2.2252	5.17	−43.90	−546.35
1a	$2NOO_w$	2.0586	2.0632	2.2172	0.38	−36.21	−553.92
1b	$2N2OO_w$	2.0516	2.1222	2.2579	−21.14	127.81	−470.41
0x	N3O	2.0762	2.1217	2.3053	80.38	188.20	−361.24
1a	$N3OO_w$	2.0122	2.2425	2.2847	−59.69	−168.37	383.37
1b	$N3OO_w$	2.0948	2.0949	2.3072	95.16	105.94	−438.09

[a]The data for pH 6.0 are reported in ref 31. [b]The **g** and **A** tensors were calculated with the non-empirical hybrid functional PBE0. The experimental **A** tensor components are reported in MHz and in parentheses, in 10^{-4} cm^{-1}. The experimental values are reported at different pH values, and the 3NO, 2N2O, and N3O models are labeled (ID) as described in the text.

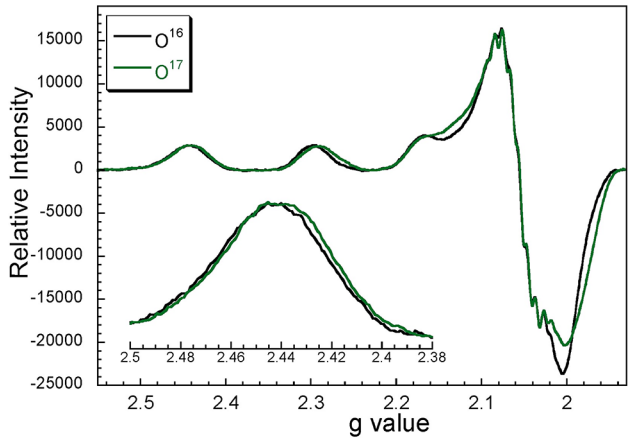

Figure 4. Comparison of X-band EPR spectra of the Cu(II) complex with PrP(92−96) at pH 7.0, prepared in ^{16}O (black) and ^{17}O water (green). Spectra were collected under the conditions specified in the experimental section at 150 K.

Thr95, and the backbone carbonyl oxygen of Gly93 (Figure 5B). The optimized structure, labeled 0x in Figure 7, shows a Cu atom in a less planar geometry than that obtained for the 4N coordination mode, with the oxygen atom of the carbonyl out of the plane formed by the three nitrogen atoms. The calculated EPR parameters for this model (Table 2) deviate considerably from the experimental values at pH 7.0, particularly for A_{zz}, indicating that this model does not reflect the chemical environment and the electronic structure of the complex. On the other hand, in the calculated absorption spectrum depicted in Figure 8, the intensities of the electronic transitions are smaller than those in the 4N mode and the d−d manifold is centered at 14119 cm^{-1} (blue line in Figure 8A), which is at lower energy than that obtained in the 4N coordination mode (Figure 6A). Additionally, in the CD spectrum, the d−d region shows a low energy transition at 12134 cm^{-1} with negative rotational strength and another at 19414 cm^{-1} with positive rotational strength (blue line in Figure 8B), behavior that is similar to that observed in the experimental CD spectrum (Figure 3D). Therefore, the computed UV−vis absorption and CD spectra (Figure 8) of this model reproduce the trends observed in the experimental data and strengthen the existence of this coordination mode at pH 7.0.

Previous electronic structure studies of the binding of Cu(II) to PrP^C have demonstrated that the best agreement between computed and experimental EPR parameters for models with a 3NO coordination mode are obtained after the inclusion of explicit water molecules.[35,37,74] Thus, to include this micro-solvation environment, we added explicit water molecules to the 0x structure in a sequential manner. The addition was done along the axial position of each side of the plane formed by the equatorial ligands, and to distinguish between them, we defined the top side as the side where the Thr95 side chain is located

dx.doi.org/10.1021/jp310000h | J. Phys. Chem. B 2013, 117, 789−799

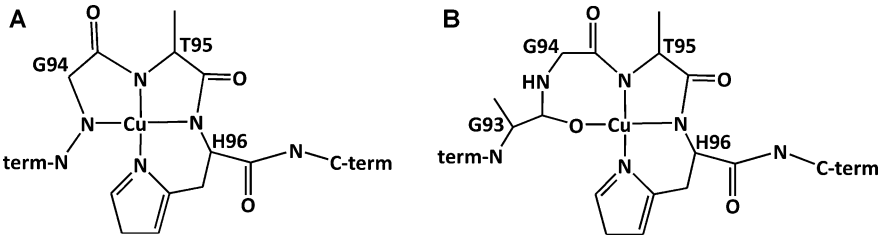

Figure 5. Coordination modes of the Cu(II) complex with PrP(92−96) corresponding to the 4N (A) and 3NO (B) models.

Table 3. Optimized Structure, β-LUMO, and Some Geometrical Parameters of the Cu(II)−PrP(92−96) Complex with a 4N Coordination Mode[a]

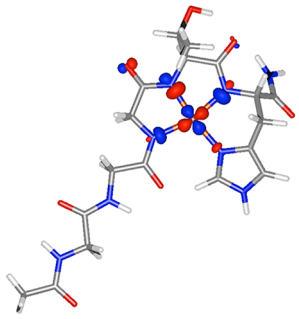

	LDA	PBE
Bond (Å)		
Cu-N1 Im	1.95	2.03
Cu-N2 H96	2.02	2.07
Cu-N3 T95	1.90	1.94
Cu-N4 G94	2.03	2.08
Angle (°)		
N1-Cu-N2	91.17	90.70
N2-Cu-N3	81.21	80.75
N3-Cu-N4	82.59	81.96
N4-Cu-N1	104.88	106.53
N1-Cu-N3	172.20	171.44
N2-Cu-N4	163.27	162.17

[a]The depicted structure and orbital were obtained with the PBE functional.

Table 4. Ligand Field Transitions for the Cu(II)−PrP(92−96) Complex with a 4N Coordination Mode Calculated with the PBE0 Functional[a]

transition	E (cm^{-1})	f (×10^{-3})	R (1e40*sgs)	% Cu I. O.
1	16906.5	0.8	−5.51919	3.4
2	17357.8	0.0	0.42974	75.0
3	18761.1	0.1	−0.16846	46.1
4	20107.5	3.3	7.63231	36.8

[a]f = oscillator strength, R = rotational strength, % Cu I. O. = percentage of copper atom in the initial orbital with the largest participation in the transition.

and the bottom side as the opposite side. Each added water molecule was placed at 2.00 Å from the metallic center.

The structure derived from model 0x after adding one water molecule in the top side has the water molecule coordinated equatorially (Figure 7, 1b), while addition of water on the bottom side leads to a structure where the water molecule is not bonded to Cu (Figure 7, 1a). The 1b structure can be discarded because the experimental results discussed in section III.1 do not support equatorial water coordination. Indeed, the calculated g_{zz} for structure 1b is too far away from the experimental value (Table 2). Thus, the second water molecule was added only to model 1a, yielding structures with a 3NO coordination and with the water molecules located in the solvation shell of the metallic center but not coordinating directly to the Cu atom (Figure 7, 2a and 2b). The incorporation of a third water molecule to 2a and 2b yields four structures (Figure 7, 3a−d). If the addition is done on the top side, one of the water molecules always optimizes as a ligand to Cu (Figure 7, 3a and 3c). In structure 3c, the water is coordinated axially, yielding a square pyramidal geometry, while, in structure 3a, the Cu−O_{water} bond is not oriented perpendicularly with respect to the 3NO plane, producing a distorted geometry with an O−Cu−O angle of 88.65°; we will refer to this coordinated water as a pseudoaxial water molecule. In contrast, if the water is added on the bottom side, the optimized structures have a 3NO mode and no water molecule is coordinated to the metal ion (Figure 7, 3b and 3d). Interestingly, the 3a and 3d models are the lowest energy structures for the series with three explicit water molecules and, consequently, they were the only geometries that were used to incorporate a fourth water molecule. Adding a fourth water molecule to the 3a and 3d models yields structures 4a−d in Figure 7. If the water molecule is added on the same side where the pseudoaxial water is coordinated to Cu (structure 3a), the Cu−OH_2 bond breaks (Figure 7, 4a); this situation is probably due to the formation of a hydrogen-bond network that pulls out the pseudoaxially coordinated water from the metallic center. On the contrary, the addition on the bottom side yields a structure that is very similar to the 3a model (Figure 7, 4b). Finally, the fourth water added to structure 3d on the top side

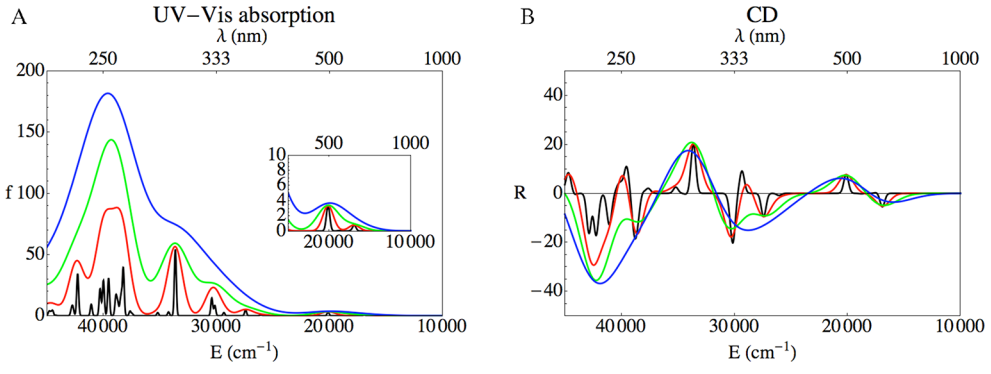

Figure 6. Computed UV−vis absorption (A) and CD (B) spectra of the Cu(II)−PrP(92−96) complex with a 4N coordination mode calculated with the PBE0 functional. The simulation was done with a fwhm of 500 (black line), 1500 (red line), 3000 (green line), and 5000 cm^{-1} (blue line).

dx.doi.org/10.1021/jp310000h | J. Phys. Chem. B 2013, 117, 789−799

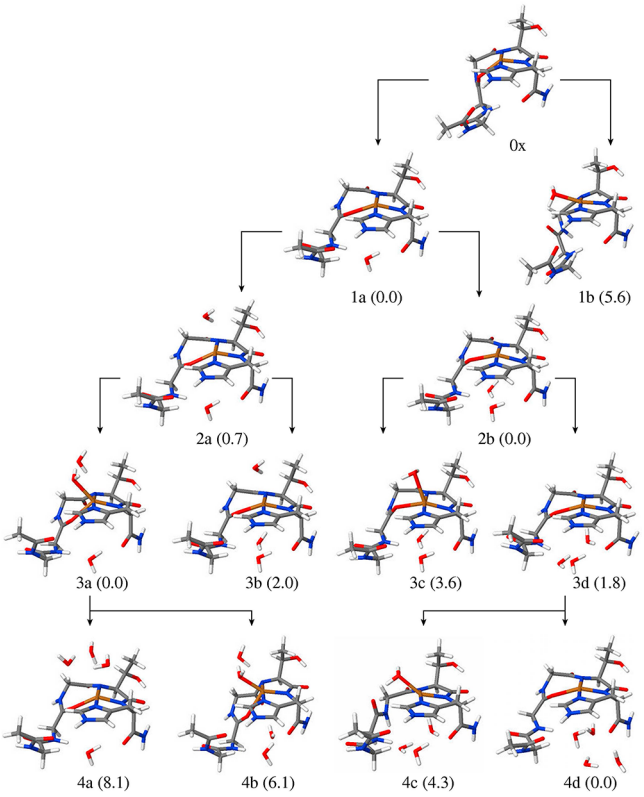

Figure 7. Optimized structures using the PBE functional of the Cu(II)−PrP(92−96) complex with 3NO coordination and with different numbers (0−4) of explicit water molecules. The numbers in parentheses are the relative energies in kcal/mol within each series.

generates a pentacoordinated Cu with a pseudoaxial water molecule (Figure 7, 4c). The lowest energy structure of the series with four water molecules is obtained after adding a water molecule on the bottom side of model 3d (Figure 7, 4d). Thus, it can be concluded that, at least for the number of explicit water molecules that we considered in this work, water binds to the copper ion on the side where the Thr95 residue is located and not on the other side, if it binds at all.

The EPR parameters of all structures shown in Figure 7 were computed and are reported in Table 2. The best agreement with the experimental g_{zz} and A_{zz} values at pH 7.0 is achieved by structures 3b and 4b, with 3NO and $3NOO_w$ coordination modes, respectively. The absorption and CD spectra for most of the structures shown in Figure 7 are depicted in Figure 9. The CD spectra of all structures with a water molecule directly coordinated to Cu equatorially (structure 1b) or axially (structures 3a, 3c, and 4b) show the larger deviations from the experimental spectrum (Figure 9D). In contrast, all structures with a 3NO coordination mode where the oxygen comes from a carbonyl group of the backbone and no explicit water molecule is coordinated to the metal ion yield the distinctive signature of the experimental CD spectrum, having a negative rotational strength at low energy (between 12000 and 15000 cm^{-1}) followed by a positive signal at higher energy (between 19000 and 21000 cm^{-1}), as can be seen in Figure 9B and Table 5. Therefore, structure 4b, having a $3NOO_w$ coordination mode, is discarded, since it does not reproduce the experimental CD spectrum (cyan line, Figure 9D). The differences between the computed g_{zz} and A_{zz} values for structure 3b and the experimental values are only 0.03 and 40 MHz, respectively, which is reasonable for this type of calculations.[37,71−73] It should be noted that, although the best agreement with experiment is achieved by structure 3b, other 3NO geometries with no water coordinating to the metal ion, such as 3d and 4d, give reasonable results too. In fact, structure 4d has the lowest energy of its series. Thus, these results indicate that the structural models that best reproduce the experimental data are those with a 3NO coordination mode and no water molecule directly bonded to the Cu ion.

III.2.3. 2N2O and N3O Coordination Modes. A proton equilibrium for the Cu(II)−PrP(92−96) complex with a pK_a of 6.3 has been identified (Figure 2), and at low pH (pH < 7), the presence of Cu(II) complexes with fewer nitrogen-based ligands has been evidenced by EPR[31] (Table 2). Thus, we also studied structural models with 2N2O and N3O coordination modes. In the 2N2O model, the Cu ion is coordinated to the imidazole nitrogen, a deprotonated amide of the His96, and the backbone carbonyl oxygens of the Gly94 and the terminal residue, in an almost square planar geometry (Figure 10, 0x). The TD-DFT calculated CD spectrum for this model (Supporting Information, Figure S2) is completely different from the experimental CD spectra in the range of pH 6 to 7 (Figure 2). To consider the effect of microsolvation, one water molecule was added in the top and bottom sides of 0x, as was done in the 3NO case. The optimized geometries have 2NOOw and 2N2OOw coordination modes, respectively (Figure 10, 1a and 1b). Table 2 shows the calculated EPR

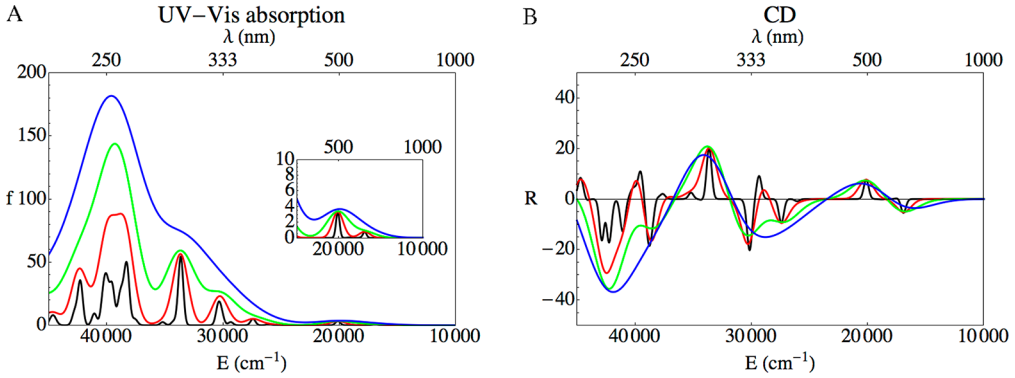

Figure 8. Computed UV−vis absorption (A) and CD (B) spectra of the Cu(II)−PrP(92−96) complex with a 3NO coordination mode in the structure 0x calculated with the PBE0 functional. The simulation was done with a fwhm of 500 (black line), 1500 (red line), 3000 (green line), and 5000 cm^{-1} (blue line).

dx.doi.org/10.1021/jp310000h | J. Phys. Chem. B 2013, 117, 789−799

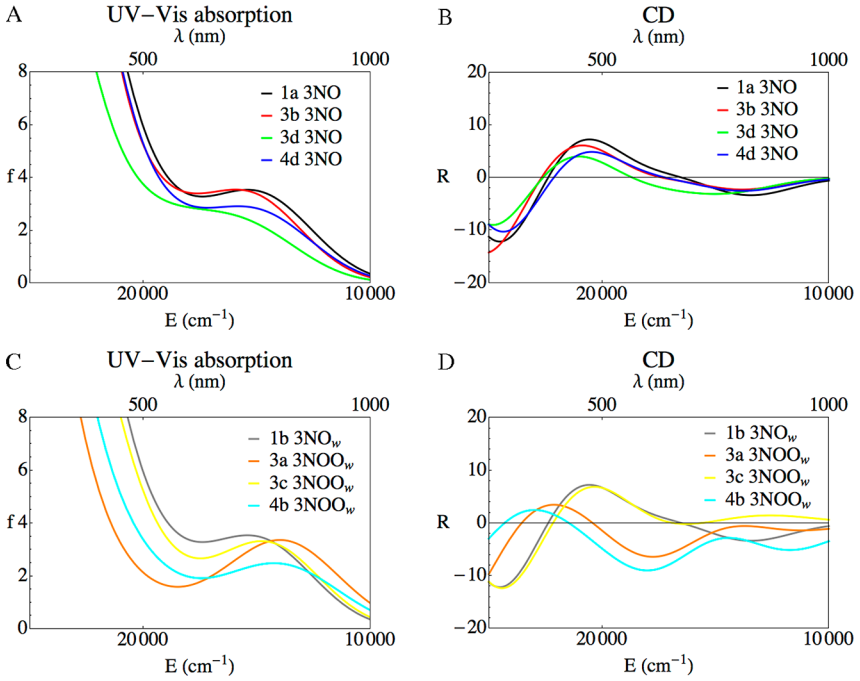

Figure 9. Computed UV−vis absorption (A, C) and CD (B, D) spectra of the different 3NO coordination modes for the Cu(II)−PrP(92−96) complex with explicit water molecules, as calculated with the PBE0 functional. The simulation was done with a fwhm of 5000 cm^{-1}.

Table 5. Energy and Sign of the Most Intense Transitions in the UV−Vis Absorption and CD d−d Region Simulated with fwhm = 5000 cm^{-1} for the Different 3NO Coordination Modes (CM) Considered for the Cu(II)−PrP(92−96) Complex[a]

		E (cm^{-1})/λ (nm)		
ID	CM	UV−vis	CD	
0x	3NO	14119/708	(−)12134/824	(+)19414/515
1a	3NO	15411/649	(−)13444/744	(+)20563/486
1b	$3NO_w$	16582/603	(−)17290/578	(+)23557/425
3a	$3NOO_w$	13976/716	(−)11215/892	(−)17762/563
3b	3NO	15930/628	(−)13826/723	(+)20873/479
3c	$3NOO_w$	14808/675	(+)12596/794	(+)20341/492
3d	3NO	17024/587	(−)15029/665	(+)21013/476
4b	$3NOO_w$	14241/702	(−)11719/853	(−)18012/555
4d	3NO	15829/632	(−)13784/725	(+)20463/489

[a]The labels (ID) are described in the text.

parameters of the 2N2O coordination models. There is no experimental EPR data for the 2N2O coordination mode, as the pK_a associated to the N3O to 2N2O conversion is 6.0, while that associated to the 2N2O to 3NO conversion is 6.3.[31] However, the EPR parameters for the 2N2O must lie between those associated to the 3NO and those for the N3O mode, i.e., 2.23 < g_{zz} < 2.36 and 541 MHz > A_{zz} > 421 MHz (Table 2). Using these criteria, structure 1b provides the best description for the 2N2O component, with a 2N2OOw coordination mode in a square-pyramidal geometry.

In the N3O model, the Cu ion is coordinated to the imidazole nitrogen of the His96, the backbone carbonyl oxygens of Thr95 and Gly94, and the terminal carbonyl group (Figure 11, 0x). The TD-DFT calculated CD spectrum for this model (Supporting Information, Figure S3) resembles the shape of the experimental CD spectrum in the range of pH 6 to 7 (Figure 2). The addition of one water molecule produces

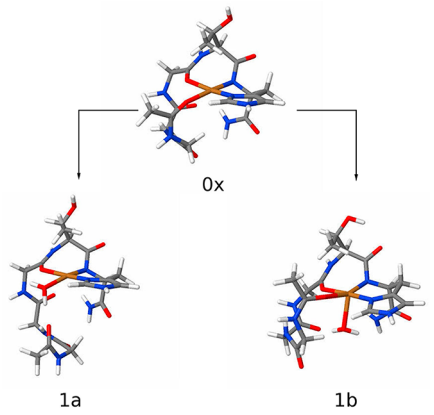

Figure 10. Optimized structures using the PBE functional of the Cu(II)−PrP(92−96) complex with a 2N2O coordination mode with (1a and 1b) and without (0x) an explicit water molecule.

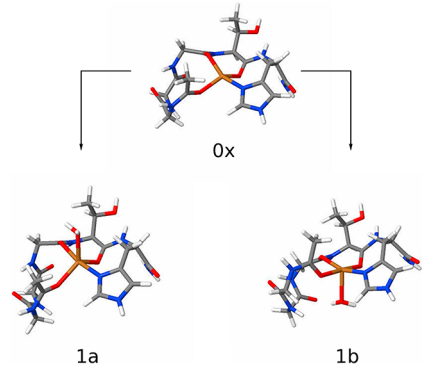

Figure 11. Optimized structures using the PBE functional of the Cu(II)−PrP(92−96) complex with a N3O coordination mode with (1a and 1b) and without (0x) an explicit water molecule.

dx.doi.org/10.1021/jp310000h | J. Phys. Chem. B 2013, 117, 789−799

pentacoordinated structures with a water molecule coordinated axially to the Cu ion (Figure 11, 1a and 1b). The computed EPR parameters for the N3O models are listed in Table 2. The best agreement with the experimental values is achieved by the 1b structure, which has a more planar geometry. Thus, the best description for the N3O component present at low pH is given by structure 1b in Figure 11. It should be noted that the chelate effect arising from the formation of ring structures in this model may be too small to compete with water molecules in the coordination sphere of the Cu(II) ion. Thus, at this point, we cannot discard the possibility that the addition of more explicit water molecules may lead to an even better description of this coordination mode.

IV. CONCLUSIONS

Copper coordination to the PrP(92−96) fragment is a pH-dependent process that at physiological pH can be described as an equilibrium between two coordination modes with a pK_a of 7.7. In one of them, the metal ion is coordinated to four equatorial nitrogens, while in the protonated form of the complex the copper atom binds equatorially to three nitrogens and one oxygen. At lower pH, experimental evidence for other coordination modes with lower content of nitrogen-based ligands, such as 2N2O and N3O, has been provided.[31] However, no crystal structures for these complexes have been obtained to date. In this study, we aimed to obtain a structural description for the different protonation states of the Cu(II)−PrP(92−96) complex, through the correlation of electronic structure calculations and spectroscopy. We have also evaluated the possibility of having water molecules as ligands to the copper ion. EPR experiments with ^{17}O-enriched water show that water molecules do not participate as equatorial ligands in the 3NO coordination mode. Consistently, DFT calculations show that, for the 4N and 3NO coordination modes, all the ligands are provided by the peptide backbone, and the models that represent the best description for these coordination modes do not involve the participation of water molecules as ligands to the copper ion. In contrast, the best models for the 2N2O and N3O involve the coordination of an axial water molecule, in a pentacoordinated square-pyramidal geometry.

Our study shows that microsolvation is crucial to achieve a good agreement between computed EPR and CD spectra and experimental data, even in the cases where the water molecules do not coordinate directly to the metal ion. These results underscore the importance of including water molecules in the structure, and indicate that implicit solvation is not sufficient to reproduce the spectroscopic features of divalent copper ions coordinated to peptides. The importance of including explicit water molecules when modeling copper binding sites in PrP^C has also become evident from theoretical studies of copper bound to the octerepeat region.[35] Understanding the role of water molecules in these copper coordination sites may also provide further insight into their redox properties and the functional implications of copper−PrP^C interactions.

Finally, this work also shows that, by combining the efforts of experimental and theoretical methodologies, it is possible to characterize structurally copper−peptide complexes, for which an X-ray crystal structure is difficult or impossible to obtain.

■ ASSOCIATED CONTENT

Ⓢ Supporting Information

EPR spectra at different pH values and UV−vis and CD simulated spectra of the 2N2O and N3O coordination modes. This material is available free of charge via the Internet at http://pubs.acs.org.

■ AUTHOR INFORMATION

Notes

The authors declare no competing financial interest.

■ ACKNOWLEDGMENTS

We thank DGSCA-UNAM, LSVP-UAMI, and CGSTIC-Cinvestav-IPN for providing us computing time in their servers KanBalam, Aitzaloa, and Xiuhcoatl, respectively. R.G.-A. and L.R.-A. thank CONACYT for PhD and postdoc fellowships, respectively. This research was funded by CONACYT (Grant Nos. 128369 and 128255 to A.V. and L.Q., respectively).

■ REFERENCES

(1) Prusiner, S. B. *Science* **1982**, *216*, 136−144.
(2) Prusiner, S. B. *Science* **1991**, *252*, 1515−1522.
(3) Prusiner, S. B. *Science* **1997**, *278*, 245−251.
(4) Davies, P.; Brown, D. R. *Biochem. J.* **2008**, *410*, 237−244.
(5) Brown, D. R.; Qin, K. F.; Herms, J. W.; Madlung, A.; Manson, J.; Strome, R.; Fraser, P. E.; Kruck, T.; vonBohlen, A.; SchulzSchaeffer, W.; et al. *Nature* **1997**, *390*, 684−687.
(6) Pauly, P. C.; Harris, D. A. *J. Biol. Chem.* **1998**, *273*, 33107−33110.
(7) Sumudhu, W.; Perera, S.; Hooper, N. M. *Curr. Biol.* **2001**, *11*, 519−523.
(8) Klamt, F.; Dal-Pizzol, F.; da Frota, M. L. C.; Walz, R.; Andrades, M. E.; da Silva, E. G.; Brentani, R. R.; Izquierdo, I.; Moreira, J. C. F. *Free Radical Biol. Med.* **2001**, *30*, 1137−1144.
(9) Nadal, R. C.; Abdelraheim, S. R.; Brazier, M. W.; Rigby, S. E. J.; Brown, D. R.; Viles, J. H. *Free Radical Biol. Med.* **2007**, *42*, 79−89.
(10) Brown, D. R.; Wong, B. S.; Hafiz, F.; Clive, C.; Haswell, S. J.; Jones, I. M. *Biochem. J.* **1999**, *344*, 1−5.
(11) Mange, A.; Milhavet, O.; Umlauf, D.; Harris, D.; Lehmann, S. *FEBS Lett.* **2002**, *514*, 159−162.
(12) Mouillet-Richard, S.; Ermonval, M.; Chebassier, C.; Laplanche, J. L.; Lehmann, S.; Launay, J. M.; Kellermann, O. *Science* **2000**, *289*, 1925−1928.
(13) Bounhar, Y.; Zhang, Y.; Goodyer, C. G.; LeBlanc, A. *J. Biol. Chem.* **2001**, *276*, 39145−39149.
(14) You, H.; Tsutsui, S.; Hameed, S.; Kannanayakal, T. J.; Chen, L.; Xia, P.; Engbers, J. D. T.; Lipton, S. A.; Stys, P. K.; Zamponi, G. W. *Proc. Natl. Acad. Sci. U.S.A.* **2012**, *109*, 1737−1742.
(15) Donne, D. G.; Viles, J. H.; Groth, D.; Mehlhorn, I.; James, T. L.; Cohen, F. E.; Prusiner, S. B.; Wright, P. E.; Dyson, H. J. *Proc. Natl. Acad. Sci. U.S.A.* **1997**, *94*, 13452−13457.
(16) Aronoff-Spencer, E.; Burns, C. S.; Avdievich, N. I.; Gerfen, G. J.; Peisach, J.; Antholine, W. E.; Ball, H. L.; Cohen, F. E.; Prusiner, S. B.; Millhauser, G. L. *Biochemistry* **2000**, *39*, 13760−13771.
(17) Burns, C. S.; Aronoff-Spencer, E.; Legname, G.; Prusiner, S. B.; Antholine, W. E.; Gerfen, G. J.; Peisach, J.; Millhauser, G. L. *Biochemistry* **2003**, *42*, 6794−6803.
(18) Jackson, G. S.; Murray, I.; Hosszu, L. L. P.; Gibbs, N.; Waltho, J. P.; Clarke, A. R.; Collinge, J. *Proc. Natl. Acad. Sci. U.S.A.* **2001**, *98*, 8531−8535.
(19) Klewpatinond, M.; Davies, P.; Bowen, S.; Brown, D. R.; Viles, J. H. *J. Biol. Chem.* **2008**, *283*, 1870−1881.
(20) Qin, K. F.; Yang, Y.; Mastrangelo, P.; Westaway, D. *J. Biol. Chem.* **2002**, *277*, 1981−1990.
(21) Chattopadhyay, M.; Walter, E. D.; Newell, D. J.; Jackson, P. J.; Aronoff-Spencer, E.; Peisach, J.; Gerfen, G. J.; Bennett, B.; Antholine, W. E.; Millhauser, G. L. *J. Am. Chem. Soc.* **2005**, *127*, 12647−12656.
(22) Burns, C. S.; Aronoff-Spencer, E.; Dunham, C. M.; Lario, P.; Avdievich, N. I.; Antholine, W. E.; Olmstead, M. M.; Vrielink, A.; Gerfen, G. J.; Peisach, J.; et al. *Biochemistry* **2002**, *41*, 3991−4001.

(23) Berti, F.; Gaggelli, E.; Guerrini, R.; Janicka, A.; Kozlowski, H.; Legowska, A.; Miecznikowska, H.; Migliorini, C.; Pogni, R.; Remelli, M.; et al. *Chem.—Eur. J.* **2007**, *13*, 1991−2001.
(24) Di Natale, G.; Osz, K.; Nagy, Z.; Sanna, D.; Micera, G.; Pappalardo, G.; Sovago, I.; Rizzarell, E. *Inorg. Chem.* **2009**, *48*, 4239−4250.
(25) Osz, K.; Nagy, Z.; Pappalardo, G.; Di Natale, G.; Sanna, D.; Micera, G.; Rizzarelli, E.; Sovago, I. *Chem.—Eur. J.* **2007**, *13*, 7129−7143.
(26) Remelli, M.; Valensin, D.; Bacco, D.; Gralka, E.; Guerrini, R.; Migliorini, C.; Kozlowski, H. *New J. Chem.* **2009**, *33*, 2300−2310.
(27) Shearer, J.; Soh, P. *Inorg. Chem.* **2007**, *46*, 710−719.
(28) Thompsett, A. R.; Abdelraheim, S. R.; Daniels, M.; Brown, D. R. *J. Biol. Chem.* **2005**, *280*, 42750−42758.
(29) Walter, E. D.; Stevens, D. J.; Spevacek, A. R.; Visconte, M. P.; Rossi, A. D.; Millhauser, G. L. *Curr. Protein Pept. Sci.* **2009**, *10*, 529−535.
(30) Klewpatinond, M.; Viles, J. H. *Biochem. J.* **2007**, *404*, 393−402.
(31) Hureau, C.; Charlet, L.; Dorlet, P.; Gonnet, F.; Spadini, L.; Anxolabehere-Mallart, E.; Girerd, J. J. *J. Biol. Inorg. Chem.* **2006**, *11*, 735−744.
(32) Hureau, C.; Mathe, C.; Faller, P.; Mattioli, T. A.; Dorlet, P. *J. Biol. Inorg. Chem.* **2008**, *13*, 1055−1064.
(33) Barry, S. D.; Rickard, G. A.; Pushie, M. J.; Rauk, A. *Can. J. Chem.* **2009**, *87*, 942−953.
(34) Pushie, M. J.; Vogel, H. J. *J. Toxicol. Environ. Health* **2009**, *72*, 1040−1059.
(35) Quintanar, L.; Rivillas-Acevedo, L.; Grande-Aztatzi, R.; Gómez-Castro, C. Z.; Arcos-López, T.; Vela, A. *Coord. Chem. Rev.* **2013**, *257*, 429−444.
(36) Yamamoto, N.; Kuwata, K. *J. Biol. Inorg. Chem.* **2009**, *14*, 1209−1218.
(37) Rivillas-Acevedo, L.; Grande-Aztatzi, R.; Lomelí, I.; García, J. E.; Barrios, E.; Teloxa, S.; Vela, A.; Quintanar, L. *Inorg. Chem.* **2011**, *50*, 1956−1972.
(38) Schaftenaar, G.; Noordik, J. H. *J. Comput.-Aided Mol. Des.* **2000**, *14*, 123−134.
(39) Kohn, W.; Sham, L. J. *Phys. Rev.* **1965**, *140*, A1133−A1138.
(40) Koster, A. M.; et al. *deMon2k*; The International deMon Developers Community, Cinvestav: Mexico D. F., Mexico, 2009.
(41) Dirac, P. A. M. *Proc. Cambridge Philos. Soc.* **1930**, *26*, 376−385.
(42) Vosko, S. H.; Wilk, L.; Nusair, M. *Can. J. Phys.* **1980**, *58*, 1200−1211.
(43) Perdew, J. P.; Burke, K.; Ernzerhof, M. *Phys. Rev. Lett.* **1996**, *77*, 3865−3868.
(44) Perdew, J. P.; Schmidt, K. In *Density Functional Theory and Its Applications to Materials*; Doren, V. V., Alsenoy, C. V., Eds.; AIP: Melville, NY, 2001.
(45) Godbout, N.; Salahub, D. R.; Andzelm, J.; Wimmer, E. *Can. J. Chem.* **1992**, *70*, 560−571.
(46) Dunlap, B. I.; Connolly, J. W. D.; Sabin, J. R. *J. Chem. Phys.* **1979**, *71*, 3396−3402.
(47) Koster, A. M.; del Campo, J. M.; Janetzko, F.; Zuniga-Gutierrez, B. *J. Chem. Phys.* **2009**, *130*, No. 114106.
(48) Neese, F. *ORCA-an ab initio, Density Functional and Semi-empirical program package*, ver. 2.6, rev. 35; University of Bonn: Bonn, Germany, 2008.
(49) Adamo, C.; Barone, V. *J. Chem. Phys.* **1999**, *110*, 6158−6170.
(50) The ORCA basis set "CoreProp" was used. This basis is based on the TurboMole DZ basis developed by Ahlrichs and co-workers and obtained from the basis set library under ftp.chemie.unikarlsruhe.de/pub/basen.
(51) Kutzelnigg, W.; Fleischer, U.; Schindler, M. *The IGLO-Method: Ab Initio Calculation and Interpretation of NMR Chemical Shifts and Magnetic Susceptibilities*; Springer-Verlag: Heidelberg, Germany, 1990; Vol. 23.
(52) Schafer, A.; Horn, H.; Ahlrichs, R. *J. Chem. Phys.* **1992**, *97*, 2571−2577.
(53) Klamt, A.; Schuurmann, G. *J. Chem. Soc., Perkin Trans. 2* **1993**, 799−805.
(54) Sinnecker, S.; Rajendran, A.; Klamt, A.; Diedenhofen, M.; Neese, F. *J. Phys. Chem. A* **2006**, *110*, 2235−2245.
(55) McMillin, D. R. In *Physical Methods in Bioinorganic Chemistry*; Que, L. J., Ed.; University Science Books: Sausalito, CA, 2000.
(56) Solomon, E. I.; Hanson, M. A. In *Inorganic Electronic Structure and Spectroscopy*; Solomon, E. I., Lever, A. B. P., Eds.; John Wiley & Sons, Inc.: New York, 1999; pp 1−129.
(57) Johnson, M. K. In *Physical Methods in Bioinorganic Chemistry*; Que, L. J., Ed.; University Science Books: Sausalito, CA, 2000.
(58) Bryce, G. F.; Gurd, F. R. N. *J. Biol. Chem.* **1966**, *241*, 122−129.
(59) Bryce, G. F.; Roeske, R. W.; Gurd, F. R. N. *J. Biol. Chem.* **1966**, *241*, 1072−1080.
(60) Bernarducci, E.; Schwindinger, W. F.; Hughey, J. L.; Kroghjespersen, K.; Schugar, H. J. *J. Am. Chem. Soc.* **1981**, *103*, 1686−1691.
(61) Daniele, P. G.; Prenesti, E.; Ostacoli, G. *J. Chem. Soc., Dalton Trans.* **1996**, 3269−3275.
(62) Fawcett, T. G.; Bernarducci, E. E.; Kroghjespersen, K.; Schugar, H. J. *J. Am. Chem. Soc.* **1980**, *102*, 2598−2604.
(63) Osz, K.; Boka, B.; Varnagy, K.; Sovago, I.; Kurtan, T.; Antus, S. *Polyhedron* **2002**, *21*, 2149−2159.
(64) Varnagy, K.; Boka, B.; Sovago, I.; Sanna, D.; Marras, P.; Micera, G. *Inorg. Chim. Acta* **1998**, *276*, 440−446.
(65) Peisach, J.; Blumberg, W. E. *Arch. Biochem. Biophys.* **1974**, *165*, 691−708.
(66) Branden, R.; Deinum, J. *FEBS Lett.* **1977**, *73*, 144−146.
(67) Getz, D.; Silver, B. L. *J. Chem. Phys.* **1974**, *61*, 630−637.
(68) Bruschi, M.; De Gioia, L.; Mitric, R.; Bonacic-Koutecky, V.; Fantucci, P. *Phys. Chem. Chem. Phys.* **2008**, *10*, 4573−4583.
(69) Quintanar, L.; Yoon, J. J.; Aznar, C. P.; Palmer, A. E.; Andersson, K. K.; Britt, R. D.; Solomon, E. I. *J. Am. Chem. Soc.* **2005**, *127*, 13832−13845.
(70) Solomon, E. I.; Szilagyi, R. K.; George, S. D.; Basumallick, L. *Chem. Rev.* **2004**, *104*, 419−458.
(71) Neese, F. *J. Chem. Phys.* **2001**, *115*, 11080−11096.
(72) Neese, F. *J. Chem. Phys.* **2003**, *118*, 3939−3948.
(73) Patchkovskii, S.; Ziegler, T. *J. Am. Chem. Soc.* **2000**, *122*, 3506−3516.
(74) Ling, Y.; Khade, R. L.; Zhang, Y. *J. Phys. Chem. B* **2011**, *115*, 2663−2670.